Solving for $S_2^{(LL)}(f,f)$ yields

$$S_2^{(LL)}(f,f) = -j2\pi(2f)C_2Z_0^{3/2}Z_L(2f) \cdot \frac{1 + 2S_1^{(LL)}(f) + [S_1^{(LL)}(f)]^2}{Z_L(2f) + Z_0}. \quad (109)$$

Equation (109) clearly reveals how the reflection coefficient of the 1-port and the linearized impedance of the load enter into determination of the second-order response. Observe that the reflection coefficient and the linearized load impedance are functions of frequency.

In general, the nonlinear scattering functions $S_n^{(LL)} \cdot (f_1,\cdots,f_n)$ can be obtained from (102) by assuming an excitation of the form

$$\alpha^{(L)}(t) = \sum_{m=1}^{n} e^{j2\pi f_m t} \quad (110)$$

in conjunction with the harmonic input method.

## V. Conclusion

Scattering variables are convenient to use when analyzing microwave systems. This paper has demonstrated that the conventional linear scattering parameter theory is a special case of a more general theory applicable to nonlinear systems. In addition, scattering variables can be used to simplify the characterization of a nonlinear multiport when the ports are matched to the reference impedance. The nonlinear scattering functions facilitate the calculation of power in nonlinear distortion products at microwave frequencies.

## References

[1] N. Wiener, *Nonlinear Problems in Random Theory*. Cambridge, MA.: M.I.T. Press, 1959.
[2] E. Bedrosian and S. O. Rice, "The output properties of Volterra systems (nonlinear systems with memory) driven by harmonic and Gaussian inputs," *Proc. IEEE*, vol. 59, pp. 1688–1707, Dec. 1971.
[3] J. Bussgang, L. Ehrman, and J. Graham, "Analysis of nonlinear systems with multiple inputs," *Proc. IEEE*, vol. 62, pp. 1088–1119, Aug. 1974.
[4] S. Narayanan, "Application of Volterra series to intermodulation distortion analysis of transistor feedback amplifier," *IEEE Trans. Circuit Theory*, vol. CT-17, pp. 518–527, Nov. 1970.
[5] M. Brilliant, "Theory of the analysis of nonlinear systems," M.I.T. Research Lab. of Electronics, Cambridge, MA, Tech. Rep. 345, Mar. 3, 1958.
[6] E. Kuh and R. Rohrer, *Theory of Linear Active Networks*. San Francisco, CA.: Holden-Day, Inc., 1967.
[7] N. Balabanian and T. Bickart, *Electrical Network Theory*. New York: John Wiley and Sons, 1969.
[8] P. Penfield, "Exact cascading for nonlinear networks," Appendix A of RADC Technical Report 74–68, Rome Air Development Center, Rome, NY, Mar. 1974.

# Experimental and Theoretical Studies on Electromagnetic Fields Induced Inside Finite Biological Bodies

BHAG SINGH GURU, STUDENT MEMBER, IEEE, AND KUN-MU CHEN, FELLOW, IEEE

***Abstract*—The total electric field inside some simulated biological bodies induced by an electromagnetic wave has been quantified by the recently developed tensor integral equation method and measured by an insulated probe. In general, the induced electric field inside a biological body was found to be quite complicated. An excellent agreement was obtained between theory and experiment.**

## I. Introduction

IN THE STUDY of the interaction of electromagnetic radiation with biological bodies, the key physical quantity which determines the bioeffects on the body is the actual electromagnetic field induced inside the body by the incident electromagnetic wave. Since a biological body is usually a heterogeneous finite body with an irregular shape, the quantification of the internal electromagnetic fields becomes a difficult problem. For mathematical simplicity, commonly used models are the plane slab [1], [2], the sphere [3]–[5], the cylinder [6], and the spheroids [7], [8]. Although these simple models provide estimates of the internal electromagnetic fields, the results have limited applicability to the biological bodies with irregular shapes and illuminated by a microwave.

Recently, Livesay and Chen [9] have developed a theoretical method called the tensor integral equation method which can be used to quantify the internal electric field induced by an incident electromagnetic wave inside arbitrarily shaped biological bodies. This method has been utilized to quantify the induced electric field inside some simulated biological bodies illuminated by a microwave. The same induced electric field has been measured by a small insulated probe. In general, the induced electric field inside the body was found to be quite complicated even though the incident

Manuscript received October 23, 1975; revised January 19, 1976. This work was supported by the National Science Foundation under Grant ENG 74-12603.

The authors are with the Department of Electrical Engineering and Systems Science, Michigan State University, East Lansing, MI 48824.

EM wave is a simple plane wave. In this study an excellent agreement was obtained between theory and experiment. This agreement confirms the accuracy of the tensor integral equation method. In this paper an inherent experimental error associated with an implantable probe immersed in a finite biological body is also discussed.

## II. Tensor Integral Equation Method

Since the tensor integral equation method [9] has been published, only two key equations are quoted here.

If a finite biological body of arbitrary shape, with permittivity $\varepsilon(\vec{r})$, conductivity $\sigma(\vec{r})$, and permeability $\mu_0$, is illuminated in free space by an incident electromagnetic wave with an electric field $\vec{E}^i(\vec{r})$, the total induced electric field $\vec{E}(\vec{r})$ inside the body can be determined from the following tensor integral equation:

$$\left[1 + \frac{\tau(\vec{r})}{3j\omega\varepsilon_0}\right]\vec{E}(\vec{r}) - \text{PV}\int_V \tau(\vec{r}')\vec{E}(\vec{r}')\cdot\overleftrightarrow{G}(\vec{r},\vec{r}')\,dV' = \vec{E}^i(\vec{r}) \quad (1)$$

where $\tau(\vec{r}) = \sigma(\vec{r}) + j\omega(\varepsilon(\vec{r}) - \varepsilon_0)$, $\varepsilon_0$ is the free-space permittivity, the PV symbol means the principal value of the integral, $\overleftrightarrow{G}(\vec{r},\vec{r}')$ is the free-space tensor Green's function, and $V$ is the body volume.

If the body is partitioned into $N$ subvolumes or cells, and $\vec{E}(\vec{r})$ and $\tau(\vec{r})$ are assumed to be constant within each cell, (1) can be transformed into $3N$ simultaneous equations for $E_x$, $E_y$, and $E_z$ at the centers of $N$ cells by the point matching method. These simultaneous equations can be written into matrix form as

$$\begin{bmatrix}[G_{xx}] & [G_{xy}] & [G_{xz}]\\ [G_{yx}] & [G_{yy}] & [G_{yz}]\\ [G_{zx}] & [G_{zy}] & [G_{zz}]\end{bmatrix}\begin{bmatrix}[E_x]\\ [E_y]\\ [E_z]\end{bmatrix} = -\begin{bmatrix}[E_x^i]\\ [E_y^i]\\ [E_z^i]\end{bmatrix}. \quad (2)$$

The $[G]$ matrix is a $3N \times 3N$ matrix, while $[E]$ and $[E^i]$ are $3N$ column matrices expressing the total electric field and the incident electric field at the centers of $N$ cells. The elements of the $[G]$ matrix have been evaluated in [9]. Therefore, with the known incident electric field $\vec{E}^i(\vec{r})$, the total induced electric field $\vec{E}(\vec{r})$ inside the body can be obtained from (2) by inverting the $[G]$ matrix.

This method has been used to calculate the induced electric field inside a biological body illuminated by a simple plane wave. The following example is given to show the fact that the induced electromagnetic field inside of a biological body can be quite complicated even though the incident electromagnetic wave is a simple plane wave. The example is a muscle layer with dimensions of $5 \times 5 \times 0.5$ cm illuminated by a plane EM wave of 1 GHz at end-on incidence, as shown in Fig. 1. For this case the electric field of the incident wave can be divided into the symmetrical and antisymmetrical components with respect to the central axis (the $x$ axis) of the muscle layer

$$\vec{E}^i = e^{-j\beta_0 z}\hat{x} = \vec{E}_s^{\,i} + \vec{E}_a^{\,i}$$

where

$$\vec{E}_s^{\,i} = \cos\beta_0 z\hat{x}$$

$$\vec{E}_a^{\,i} = -j\sin\beta_0 z\hat{x}. \quad (3)$$

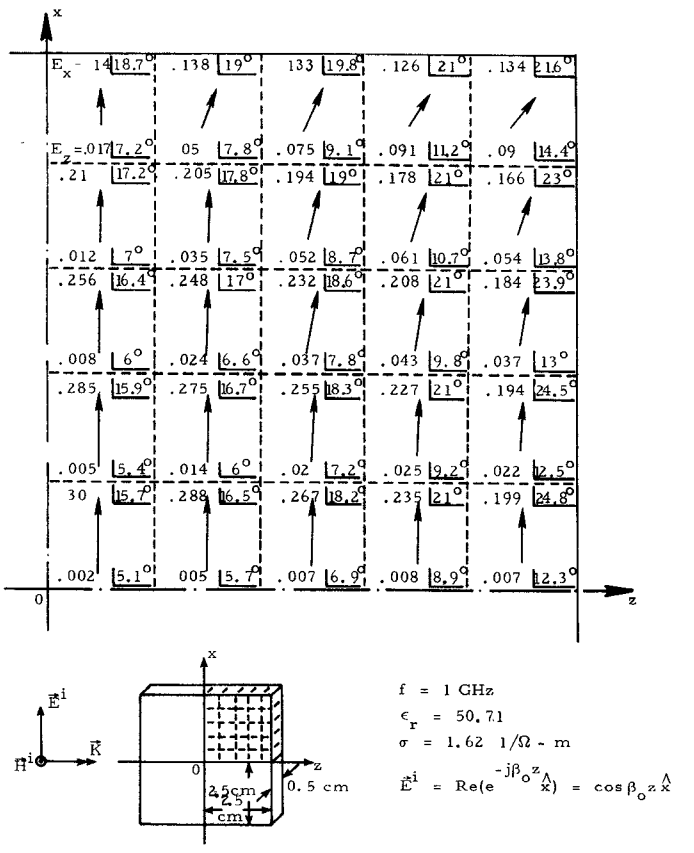


Fig. 1. The symmetrical mode of the electric field induced in a muscle layer by the symmetrical component of the electric field of an incident plane wave (only ¼ of the layer shown).

The total electric field $\vec{E}$ induced inside the muscle layer also consists of a symmetrical component $\vec{E}_s$ and an antisymmetrical component $\vec{E}_a$. $\vec{E}_s$ and $\vec{E}_a$ can be determined from the following tensor integral equations:

$$\left[1 + \frac{\tau(\vec{r})}{3j\omega\varepsilon_0}\right]\vec{E}_s(\vec{r}) - \text{PV}\int_V \tau(\vec{r}')\vec{E}_s(\vec{r}')\cdot\overleftrightarrow{G}(\vec{r},\vec{r}')\,dV' = \cos\beta_0 z\hat{x} \quad (4)$$

$$\left[1 + \frac{\tau(\vec{r})}{3j\omega\varepsilon_0}\right]\vec{E}_a(\vec{r}) - \text{PV}\int_V \tau(\vec{r}')\vec{E}_a(\vec{r}')\cdot\overleftrightarrow{G}(\vec{r},\vec{r}')\,dV' = -j\sin\beta_0 z\hat{x}. \quad (5)$$

The numerical solutions for $\vec{E}_s(\vec{r})$, $\vec{E}_a(\vec{r})$ are shown in Figs. 1–3. Fig. 1 shows $\vec{E}_s(\vec{r})$, which is roughly a linearly polarized field parallel to the incident electric field. Fig. 2 shows $\vec{E}_a(\vec{r})$, which is approximately a linearly polarized circulatory field. This $\vec{E}_a(\vec{r})$ excites a circulatory eddy current which can be considered to be induced by the magnetic field of the incident wave from an alternative viewpoint. If $\vec{E}_s(\vec{r})$ and $\vec{E}_a(\vec{r})$ are combined to yield the total electric field $\vec{E}(\vec{r})$, an elliptically polarized field is obtained, as shown in Fig. 3. In general, the amplitude and shape of $\vec{E}(\vec{r})$ is a function of location inside the body and is also dependent on the frequency and polarization of the incident wave and the electrophysical properties of the body.

It is important to point out that if the incident electric field $\vec{E}^i(\vec{r})$ were assumed to be approximately uniform over the tissue layer and the antisymmetrical component of $\vec{E}^i(\vec{r})$ were ignored (this is a careless assumption often used

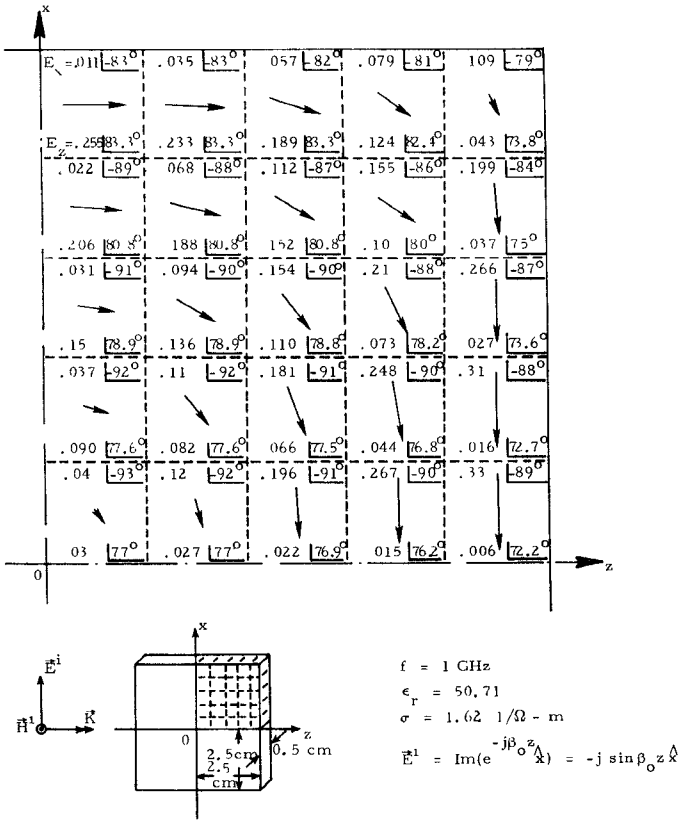


Fig. 2. The antisymmetrical mode of the electric field induced in a muscle layer by the antisymmetrical component of the electric field of an incident plane wave (only ¼ of the layer is shown).

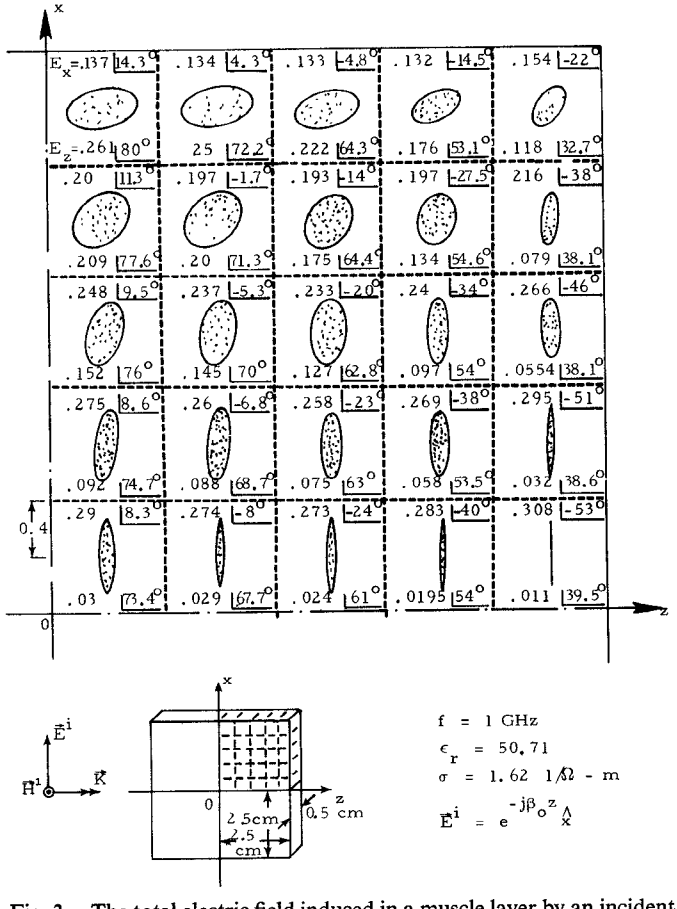


Fig. 3. The total electric field induced in a muscle layer by an incident plane wave (only ¼ of the layer is shown).

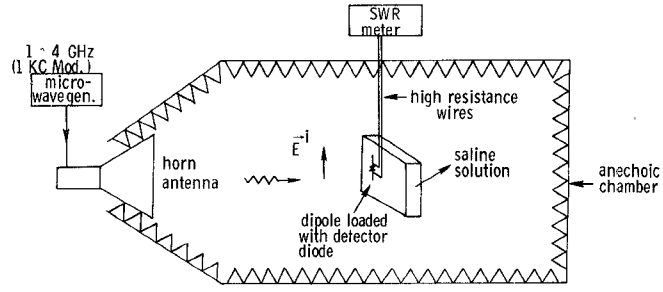


Fig. 4. Experimental setup for measurement of electric field induced inside a box filled with saline solution.

when the body is small compared to a wavelength), the total induced electric field $\vec{E}(\vec{r})$ would have been a linearly polarized field with a distribution similar to $\vec{E}_s(\vec{r})$, as shown in Fig. 1. Thus the antisymmetrical component $\vec{E}_a(\vec{r})$ would be completely overlooked and the precise nature of the elliptically polarized total electric field $\vec{E}(\vec{r})$ would never have been predicted.

This example illustrates the fact that a precise specification of the incident electric field is essential for an accurate determination of the induced electric field inside the body. Thus special care is warranted for the case of a body illuminated by a nonuniform electromagnetic field. For the case of electrically small bodies, if the quasi-static approximation is to be made, the body should be assumed to be immersed in an approximately uniform incident electric field as well as an approximately uniform incident magnetic field.

To prove the aforementioned theoretical observation and to confirm the accuracy of the tensor integral equation method, an experiment has been conducted to measure the induced electric field inside some boxes containing saline solution. The details of the experimental study are given in Section III.

## III. Experiment

The schematic diagram of the experimental setup for measuring the induced electric field in simulated biological bodies is shown in Fig. 4. For simulated biological bodies, a number of experimental models with various dimensions were constructed with plexiglass and filled with a saline solution of various salt concentrations. These models were placed in an anechoic chamber and illuminated by electromagnetic waves with frequencies ranging from 1.7 to 3.0 GHz (with 1-kHz modulation) radiated from a horn antenna. The induced electric field inside the solution was measured by a small dipole-type probe loaded with a microwave detector diode (HP 5082-2755) at the terminals. The detected output of the probe was connected to an SWR meter through a pair of thin high resistance wires (Nichrome V wire of 2-mil diameter). The high resistance lead wires were needed to minimize the interference of the wires with the incident electromagnetic wave. Since the probe and part of the lead wires were immersed in a conducting saline solution, it was necessary to insulate the probe and the lead wires with a thin layer of Klyron spray. A vertical dipole probe was used to measure the vertical component of the induced electric field ($E_x$) and a horizontal dipole probe

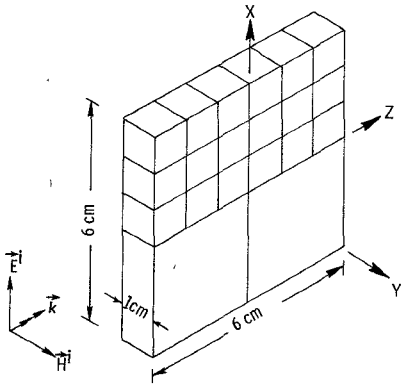


Fig. 5. A rectangular model containing salt solution illuminated by an EM wave at end-on incidence.

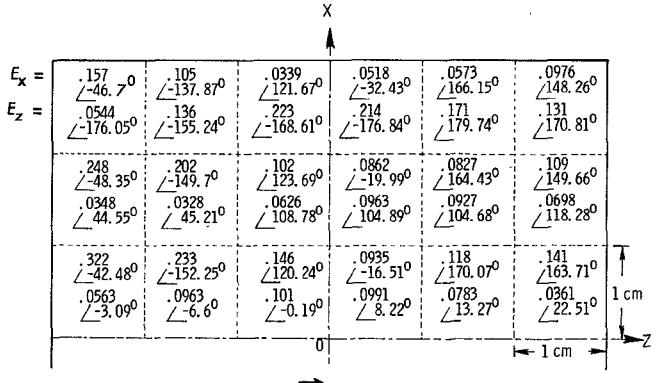


Fig. 6. Theoretically induced $\vec{E}$ field in $\frac{1}{4}$ of the rectangular shaped model shown in Fig. 5. Freq = 2.45 GHz, $\sigma$ = 5.934 ℧/m, $\varepsilon$ = 68.487 $\varepsilon_0$. Salt concentration = 0.5 normal. Cell size = 1 cm$^3$.

was used to measure the horizontal components ($E_y$ and $E_z$). The length of the dipole is about 5 mm.

The experimental results are shown in comparison with the theoretical results in Figs. 5–17. In Fig. 5 a rectangular plexiglass box with dimensions of 6 × 6 × 1 cm containing 0.5 normal saline solution is illuminated by a microwave of 2.45 GHz with a vertical electric field and at end-on incidence. Fig. 6 indicates the theoretical results for the $x$ and $z$ components of the induced $\vec{E}$ field at the centers of the cells. The $y$ component is neglected because it is very small. In the calculation, conductivity $\sigma$ is assumed to be 5.934 ℧/m and permittivity $\varepsilon$ is assumed to be 68.487$\varepsilon_0$ corresponding to a 0.5 normal salt concentration at 9.45 GHz [10]. Only a half of the model is shown in Fig. 6 because of symmetry. The upper part of Fig. 7 shows the comparison of the theoretical and experimental results for the dissipated power due to $E_x$, $\frac{1}{2}\sigma|E_x|^2$, as a function of $z$ along $x$ = 0.5 cm, $x$ = 1.5 cm, and $x$ = 2.5 cm lines. The lower part of Fig. 7 shows the theoretical and experimental values of the dissipated power due to $E_z$, $\frac{1}{2}\sigma|E_z|^2$, as a function of $z$ along $x$ = 0.5 cm, $x$ = 1.5 cm, and $x$ = 2.5 cm lines. It is observed that the patterns of the dissipated power are quite complicated functions of the location, but the agreement between the theory and the experiment is excellent. It is noted in Fig. 7 that experimental results on $\sigma/2|E_z|^2$ are not available because it was not possible to measure $E_z$ near the edge of the box with a horizontal probe of

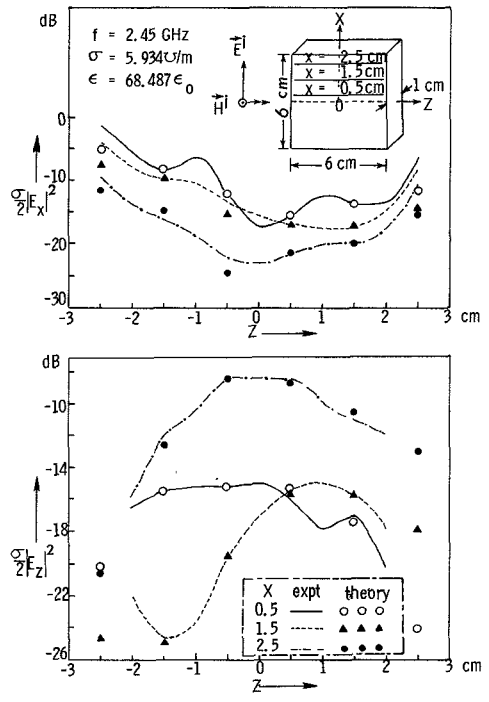


Fig. 7. Theoretical and experimental values of the dissipated power due to $E_x$ and $E_z$, i.e., $(\sigma/2)|E_x|^2$ and $(\sigma/2)|E_z|^2$, respectively, as a function of $z$ along $x$ = 0.5 cm, $x$ = 1.5 cm, and $x$ = 2.5 cm.

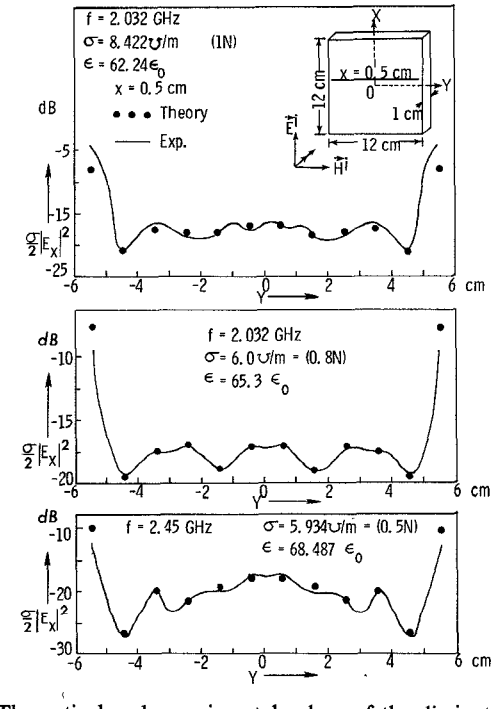


Fig. 8. Theoretical and experimental values of the dissipated power due to $E_x$, $(\sigma/2)|E_x|^2$, as a function of $y$ along $x$ = 0.5 cm, for different frequencies, conductivities, and permittivities.

finite dimensions. In the next example we consider the field inside a model with dimensions of 12 × 12 × 1 cm containing saline solutions of various salt concentrations and illuminated by a microwave of 2.032 or 2.45 GHz at normal incidence. Fig. 8 shows the theoretical and experimental values of the dissipated power due to $E_x$,

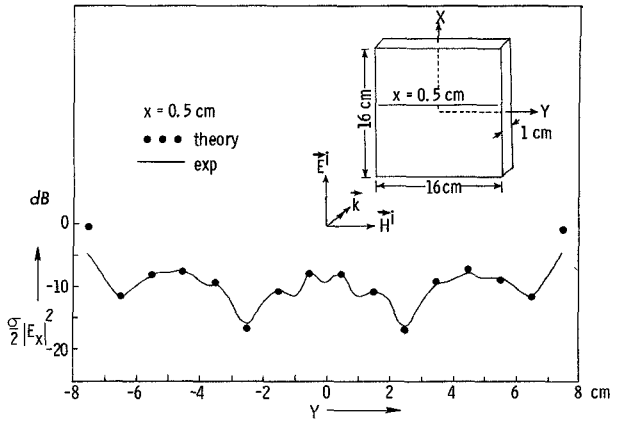


Fig. 9. Theoretical and experimental values of the dissipated power due to $E_x$, $(\sigma/2)|E_x|^2$, as a function of $y$ along $x = 0.5$ cm. Freq = 2.45 GHz, $\sigma = 5.934$ ℧/m, $\varepsilon = 68.487\ \varepsilon_0$. Salt concentration = 0.5 normal.

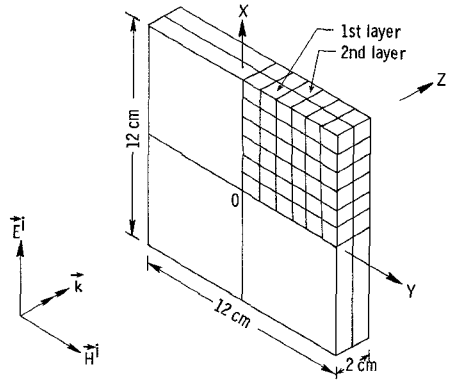


Fig. 10. A rectangular two-layer model containing salt solution illuminated by an EM wave at normal incidence.

$\frac{1}{2}\sigma|E_x|^2$, as a function of $y$ along $x = 0.5$ cm line for three cases of different frequencies, conductivities, and permittivities. For each case in Fig. 8 particular values of $f$, $\sigma$, and $\varepsilon$ are indicated. The distribution of the dissipated power is shown to change quite significantly when $f$, $\sigma$, and $\varepsilon$ are changed only slightly. The agreement between theory and experiment is excellent except at the very edge of the model. This discrepancy will be discussed in Section IV. In Fig. 9 the distribution of $\sigma/2|E_x|^2$ in a larger model with dimensions of 16 × 16 × 1 cm is shown. Relevant parameters are shown in the figure. In this figure an excellent agreement between theory and experiment is again obtained except at the edge of the model. We also considered a thicker model with dimensions of 12 × 12 × 2 cm as shown in Fig. 10. The purpose of this study is to see how the induced electric field decays as the incident wave penetrates the body and to observe the accompanied change in the field distribution pattern. Fig. 11 shows the theoretical and experimental results for the dissipated power due to $E_x$, $\sigma/2|E_x|^2$, as a function of $y$ along $x = 0.5$ cm line passing through the centers of the first and second layers. The dissipated power in the first layer is several decibels higher than that in the second layer as expected. An interesting observation, however, is that the distribution patterns of the dissipated power differ significantly in these two layers. An excellent

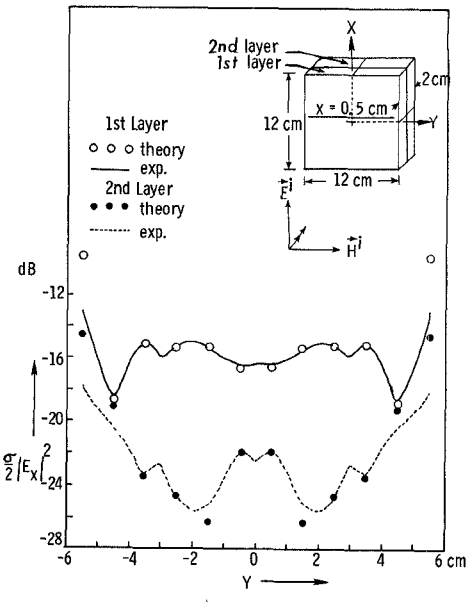


Fig. 11. Theoretical and experimental values of the dissipated power due to $E_x$, $(\sigma/2)|E_x|^2$, as a function of $y$ along $x = 0.5$ cm. Freq = 2.45 GHz, $\sigma = 5.934$ ℧/m, $\varepsilon = 68.487\ \varepsilon_0$. Salt concentration = 0.5 normal.

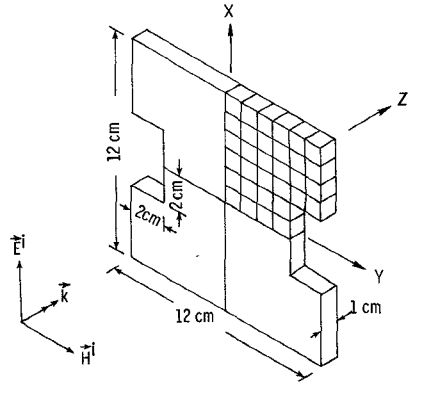


Fig. 12. An I-shaped model containing saline solution illuminated by an EM wave at normal incidence.

agreement between the theory and the experiment is also observed in this case.

After examining the induced fields inside rectangular bodies to a great extent, the case of irregular bodies is considered. An I-shaped model with dimensions as shown in Fig. 12 was constructed and was illuminated by a 2.45-GHz microwave at normal incidence and at end-on incidence. The model was filled with a saline solution of 0.5 normality in the experiment. Fig. 13 indicates the theoretical values of the induced $\vec{E}$ field inside the model when illuminated by the microwave at normal incidence. Only a quarter of the model is shown in Fig. 13 because of symmetry. The amplitude and phase angle of $E_x$ and $E_y$ at the centers of the cells are shown in this figure as well. $E_z$ is neglected because it is extremely small. Fig. 14 shows the comparison of the theoretical and experimental results for the dissipated power due to $E_x$, $\sigma/2|E_x|^2$, as a function of $y$ along $x = 0.5$ cm and $x = 3.5$ cm lines. The patterns of the dissipated power are quite complicated functions of the

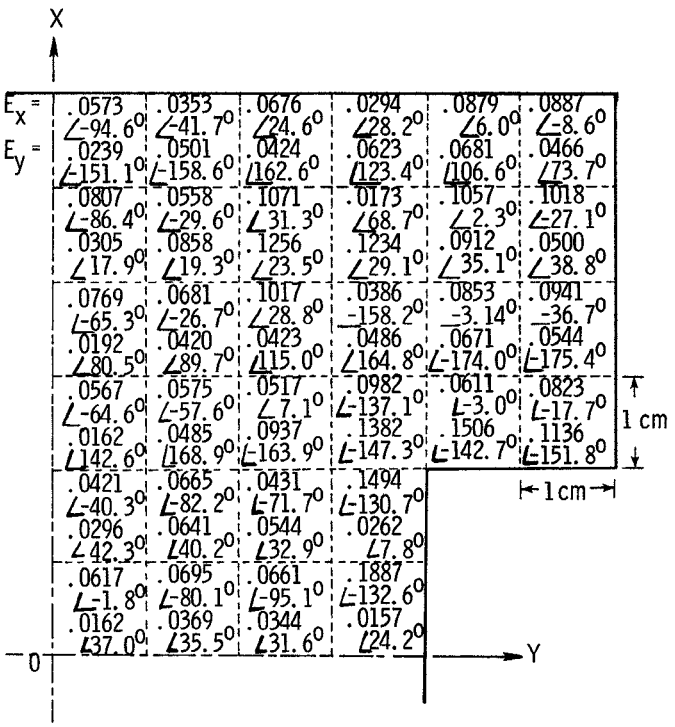


Fig. 13. Theoretically induced $\vec{E}$ field in $\frac{1}{4}$ of the I-shaped model shown in Fig. 1. Freq = 2.45 GHz, $\sigma$ = 5.934 ℧/m, $\varepsilon$ = 68.487 $\varepsilon_0$, salt concentration = 0.5 normal. Cell size = 1 cm³. Incident $E$ field: $\vec{E}^i = \hat{x}1e^{-jk0^z}$ V/m at 2.45 GHz.

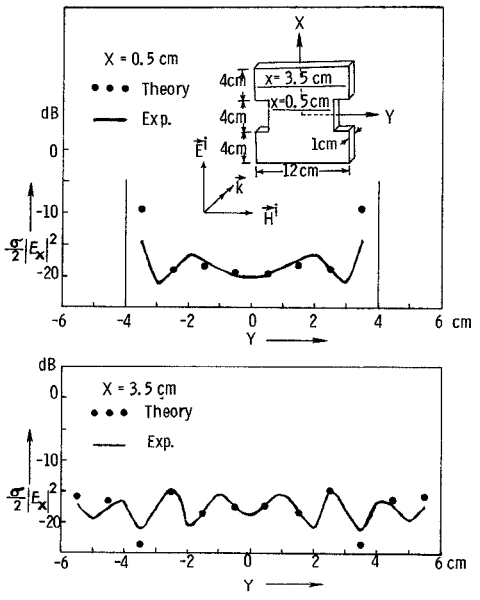


Fig. 14. Theoretical and experimental values of the dissipated power due to $E_x$, $\frac{1}{2}\sigma|E_x|^2$, as a function of $y$ along $x$ = 0.5 cm and $x$ = 3.5 cm. Freq = 2.45 GHz, $\sigma$ = 5.934 ℧/m, $\varepsilon$ = 68.487 $\varepsilon_0$. Salt concentration = 0.5 normal.

location, but the agreement between the theoretical and experimental results is excellent. Fig. 15 shows the theoretical and experimental values of the dissipated power due to $E_y$, $\sigma/2|E_y|^2$, as a function of $y$ along $x$ = 0.5 cm and $x$ = 3.5 cm lines. In Figs. 16 and 17 the results for the case of the I-shaped model illuminated by the same microwave at

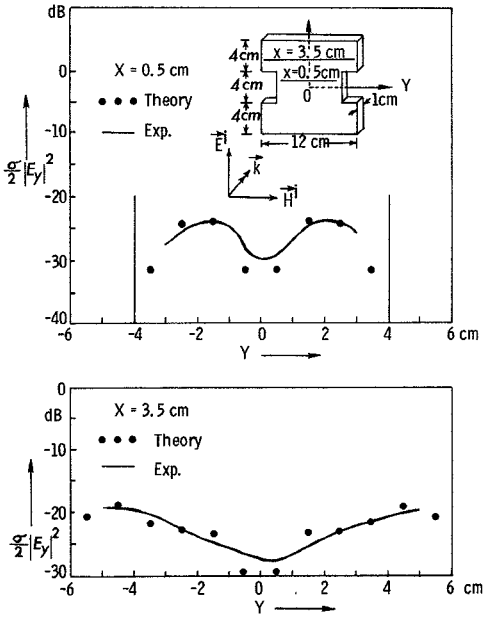


Fig. 15. Theoretical and experimental values of the dissipated power due to $E_y$, $\frac{1}{2}\sigma|E_y|^2$, as a function of $y$ along $x$ = 0.5 cm and $x$ = 3.5 cm. Freq = 2.45 GHz, $\sigma$ = 5.934 ℧/m, $\varepsilon$ = 68.487 $\varepsilon_0$. Salt concentration = 0.5 normal.

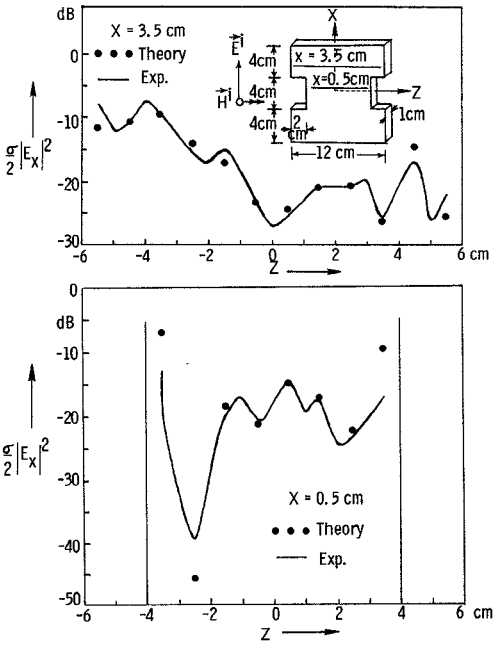


Fig. 16. Theoretical and experimental values of the dissipated power due to $E_x$, $(\sigma/2)|E_x|^2$, as a function of $Z$ along $x$ = 3.5 cm and $x$ = 0.5 cm. Freq = 2.45 GHz, $\sigma$ = 5.934 ℧/m, $\varepsilon$ = 68.487 $\varepsilon_0$. Salt concentration = 0.5 normal.

end-on incidence are shown. Fig. 16 shows the comparison of the theoretical and experimental results for the dissipated power due to $E_x$, $\sigma/2|E_x|^2$, as a function of $z$ along $x$ = 3.5 cm and $x$ = 0.5 cm lines. It is observed that the patterns of the dissipated power as functions of the location are entirely different from the case of the normal incidence. Nevertheless, an excellent agreement between theory and experiment was again obtained in this case. (It is noted

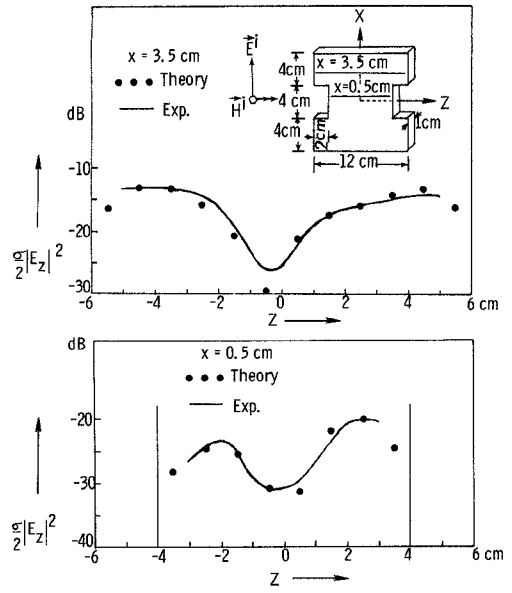


Fig. 17. Theoretical and experimental values of the dissipated power due to $E_z$, $(\sigma/2)|E_z|^2$, as a function of $z$ along $x = 3.5$ cm and $x = 0.5$ cm. Freq = 2.45 GHz, $\sigma = 5.934$ ℧/m, $\varepsilon = 68.487\ \varepsilon_0$. Salt concentration = 0.5 normal.

that in the end-on incidence case the $z$ axis corresponds to the $y$ axis of the normal incidence case.) Fig. 17 shows the theoretical and experimental values of the dissipated power due to $E_z$, $\sigma/2|E_z|^2$, as a function of $z$ along $x = 3.5$ cm and $x = 0.5$ cm lines.

As evidenced by the examples given in Figs. 5–17, the tensor integral equation method has been completely confirmed by the experiment with a minor exception at the very edge of the body. The discrepancy between theory and experiment at the edge of the body is essentially due to an inherent error in the probe measurement. This point is discussed in Section IV.

## IV. Experimental Error

When a probe is immersed in a finite biological body to measure the induced electric field, the output of the probe becomes location dependent especially at the edge of the body. To show this fact, let us consider the geometry as shown in Fig. 18. A finite body occupies a region $V$ of space and is characterized by electrical parameters $\varepsilon(\vec{r})$, $\sigma(\vec{r})$, and $\mu_0$. It is illuminated by an incident wave with an electric field $\vec{E}^i$. A thin wire probe, immersed in $V$, lies along contour $\Gamma$; location along the probe is designated by the variable $s$ with origin $s = 0$ at the probe terminals; $\hat{s}$ is a unit tangent vector to $\Gamma$ at any point. $V_0$ and $I_0$ are the voltage and current at the probe terminals, to which a load impedance $Z_L$ is connected. The incident electric field $\vec{E}^i$ excites an induced electric field $\vec{E}(\vec{r})$ in the body $V$, and this field subsequently excites a current distribution $I(s) = I_0 f(s)$ in the wire probe where $f(s)$ is a current distribution function with $f(0) = 1$. Induced probe current $I(s)$ maintains a secondary field $\vec{E}_p$ in the body. Thus the total electric field inside $V$ in the presence of the probe is

$$\vec{E}'(\vec{r}) = \vec{E}(\vec{r}) + \vec{E}_p(\vec{r}). \tag{6}$$

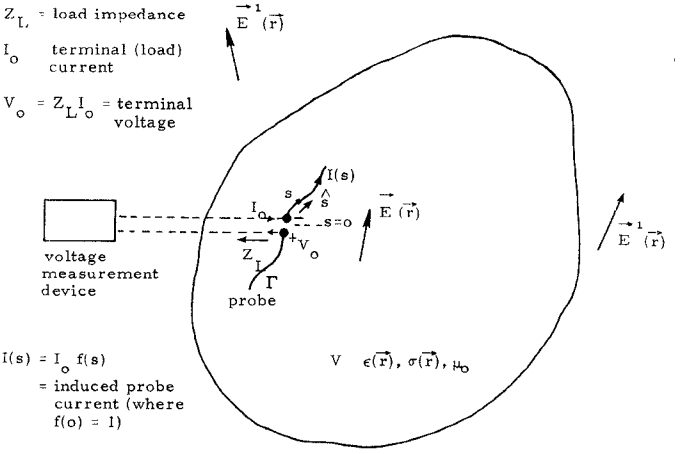


Fig. 18. Configuration of probe in a finite heterogeneous volume conductor.

The function of the probe is to measure $\vec{E}(\vec{r})$ and not $\vec{E}'(\vec{r})$. Indeed this is the case, as can be seen from the following development.

The boundary condition on a tangential electric field at the probe surface requires that $\hat{s} \cdot \vec{E}'(s) = 0$, except at the slice gap terminals

$$\hat{s} \cdot \vec{E}'(s) = V_0\delta(s) = Z_L I_0 \delta(s) \tag{7}$$

where $V_0 = Z_L I_0$, as shown in Fig. 18.

Integrating (7), we have

$$\int_\Gamma f(s)\hat{s} \cdot \vec{E}'(s)\, ds = Z_L I_0, \qquad (\because f(0) = 1). \tag{8}$$

With (6), (8) becomes

$$\int_\Gamma f(s)\hat{s} \cdot \vec{E}(s)\, ds + \int_\Gamma f(s)\hat{s} \cdot \vec{E}_p(s)\, ds = Z_L I_0. \tag{9}$$

Since the first integral of (9) represents the total driving force for the probe current, we can define an equivalent probe driving voltage as

$$V_{eq} = \int_\Gamma f(s)\hat{s} \cdot \vec{E}(s)\, ds. \tag{10}$$

It is noted that $\vec{E}(s)$ is the internal electric field at the probe location, in the absence of the probe, and is the key quantity to be measured.

The second integral of (9) is the integration of $\vec{E}_p(s)$, which is proportional to $I_0$. We can define an internal impedance for the probe as

$$Z_{in} = -\frac{1}{I_0}\int_\Gamma f(s)\hat{s} \cdot \vec{E}_p(s)\, ds. \tag{11}$$

This $Z_{in}$ is the input impedance of the probe when it is used as a radiating antenna imbedded in a finite biological body.

With (10) and (11) substituted in (9), we obtain

$$V_{eq} = I_0 Z_{in} + I_0 Z_L$$

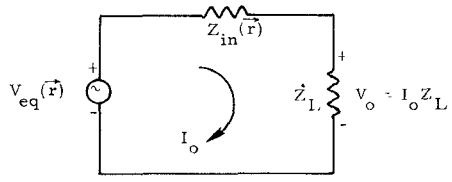


Fig. 19. Equivalent circuit for probe in a finite heterogeneous volume conductor.

or

$$I_0 = \frac{V_{eq}}{Z_{in} + Z_L}. \tag{12}$$

Equation (12) leads to an equivalent circuit for the probe, as shown in Fig. 19. This circuit differs from the conventional equivalent circuit for a receiving antenna in that $Z_{in}$ is a strong function of the heterogeneity of the medium and the body geometry, and $V_{eq}$ is also influenced by the heterogeneity of the medium because $f(s)$ is a function of electrical parameters at the probe location.

The probe response is equal to the terminal voltage and can be expressed as

$$\begin{aligned} V_0(\vec{r}) &= I_0 Z_L = \frac{V_{eq}(\vec{r}) Z_L}{Z_{in}(\vec{r}) + Z_L} \\ &= \frac{Z_L}{Z_{in}(\vec{r}) + Z_L} \int_\Gamma f(s)\hat{s} \cdot \vec{E}(s)\, ds \\ &= \vec{E}(\vec{r}) \cdot \int_\Gamma f(s)\hat{s}\, ds \left[\frac{Z_L}{Z_{in}(\vec{r}) + Z_L}\right] \end{aligned} \tag{13}$$

(for a small probe). Equation (13) clearly indicates that the probe response is proportional to the internal electric field $\vec{E}(\vec{r})$ at the probe location in the absence of the probe. However, it also shows the proportionality constant between $V_0(\vec{r})$ and $\vec{E}(\vec{r})$ to be a strong function of probe location for the following reasons. First, $Z_{in}(\vec{r})$ as defined in (11) is a function of location because $\vec{E}_p(s)$ produced by the probe current is dependent on the relative position of the probe in the body and the body geometry. Secondly, the distribution function for the probe current $f(s)$ is dependent on the electrical properties $(\varepsilon(\vec{r}),\sigma(\vec{r}))$ at the probe location. It is noted that in a homogeneous medium, such as in our experimental models, $\varepsilon$ and $\sigma$ are constant so that $f(s)$ remains constant. However, $Z_{in}(\vec{r})$ is still a strong function of the location in a homogeneous finite body.

A simple experiment can indicate that $Z_{in}(\vec{r})$ changes most rapidly near the edge of the body. Thus the proportionality constant between $V_0(\vec{r})$ and $\vec{E}(\vec{r})$ may undergo a rapid change near the edge of the body leading to an inherent experimental error at this location. Therefore a location-dependent probe calibration factor is needed before an implantable probe can be used to accurately measure the internal field induced inside a finite biological body.

## V. Conclusion

An experiment has been conducted to measure the induced electric field inside finite bodies containing saline solution with shielded implantable probes. Experimental results are used to confirm the accuracy of the theoretical results based on the tensor integral equation method. The theoretical and experimental results both indicate the complexity of the induced electric field in a finite biological body. An inherent experimental error associated with an implantable probe immersed in a finite biological body was also discussed.

In the numerical calculation of the tensor integral equation method, if the size of the cells is kept smaller than $\frac{1}{4}$ of the free-space wavelength, sufficiently accurate results are obtained. Although with this cell size it is not possible to predict the exact pattern of the standing wave inside the body, it was found to be accurate enough to predict the induced electric field at the centers of the cells. If a more accurate pattern of the standing wave is needed, it is only necessary to reduce the cell size at the expense of increasing the computing time. It is important to note that the numerical tensor integral equation method can produce exact solutions for the induced electric field in any arbitrarily shaped biological body; the only limitation is the limitation in the computing time and computer storage capacity.

## References

[1] H. P. Schwan, "Radiation biology, medical applications, and radiation hazards," in *Microwave Power Engineering*, vol. 2, E. C. Okress, Ed. New York: Academic Press, pp. 215–232, 1968.

[2] J. F. Lehmann, A. W. Guy, V. C. Johnston, G. D. Brunner, and J. W. Bell, "Comparison of relative heating patterns produced in tissues by exposure to microwave energy at frequencies of 2450 and 900 megacycles," *Arch. Phys. Med. Rehabil.*, vol. 43, pp. 69–76, Feb. 1962.

[3] A. R. Shapiro, R. F. Lutomirski, and H. T. Yura, "Induced fields and heating within a cranial structure irradiated by an electromagnetic plane wave," *IEEE Trans. on Microwave Theory and Techniques*, vol. MTT-19, no. 2, pp. 187–196, Feb. 1971.

[4] H. N. Kritikos and H. P. Schwan, "Hot spots generated in conducting spheres by electromagnetic waves and biological implications," *IEEE Trans. on Biomedical Engineering*, vol. BME-19, no. 1, pp. 53–58, Jan. 1972.

[5] J. C. Lin, A. W. Guy, and C. C. Johnson, "Power deposition in a spherical model of man exposed to 1–20 MHz electromagnetic field," *IEEE Trans. on Microwave Theory and Techniques*, vol. MTT-21, no. 12, pp. 791–797, Dec. 1973.

[6] H. S. Ho, A. W. Guy, R. A. Sigelmann, and J. F. Lehmann, "Electromagnetic heating patterns in circular cylindrical models of human tissue," in *Proc. 8th Ann. Conf. Medical and Biological Engineering*, p. 27 (Chicago, IL, July 1969).

[7] C. H. Durney, C. C. Johnson, and H. Massoudi, "Long-wavelength analysis of plane wave irradiation of a prolate spheroid model of man," *IEEE Trans. on Microwave Theory and Techniques*, vol. MTT-23, pp. 246–253, Feb. 1975.

[8] C. C. Johnson, C. H. Durney, and H. Massoudi, "Long-wavelength electromagnetic power absorption in prolate spheroidal models of man and animals," *IEEE. Trans. on Microwave Theory and Techniques*, vol. MTT-23, pp. 739–747, Sept. 1975.

[9] D. E. Livesay and K.-M. Chen, "Electromagnetic fields induced inside arbitrarily shaped biological bodies," *IEEE Trans. on Microwave Theory and Techniques*, vol. MTT-22, no. 12, pp. 1273–1280, Dec. 1974.

[10] L. K. Lapley and W. M. Adams, "Electromagnetic dispersion curves for natural waters," *Water Resource Research*, vol. 7, no. 6, pp. 1538–1547, Dec. 1971.